ACS Catalysis

Research Article

pubs.acs.org/acscatalysis

Enhancement of Solar Hydrogen Generation by Synergistic Interaction of $La_2Ti_2O_7$ Photocatalyst with Plasmonic Gold Nanoparticles and Reduced Graphene Oxide Nanosheets

Fanke Meng,[†] Scott K. Cushing,[‡] Jiangtian Li,[†] Shimeng Hao,[†] and Nianqiang Wu*[,†]

[†]Department of Mechanical and Aerospace Engineering, West Virginia University, Morgantown, West Virginia 26506-6106, United States

[‡]Department of Physics and Astronomy, West Virginia University, Morgantown, West Virginia 26506-6315, United States

Supporting Information

ABSTRACT: This report shows that incorporating nitrogen-doped $La_2Ti_2O_7$ (NLTO) photocatalyst with gold nanoparticles and reduced graphene oxide (rGO) nanosheets improves the photocatalytic hydrogen generation rate significantly. The underlying mechanism of the photocatalysis enhancement by the presence of both the Au nanoparticles and the rGO nanosheets is revealed. Nitrogen doping alone can extend the light absorption range of photocatalyst to 550 nm. In addition, nitrogen doping has enabled plasmon-induced resonance energy transfer (PIRET) from the plasmonic Au nanoparticle to NLTO, inducing charge separation in NLTO under solar radiation up to 600 nm. The Au nanoparticles not only serve as the photosensitizers but also lead to a shift in the flat band potential, suppressing the charge recombination and improving the charge extraction. The rGO does not affect the charge separation process but significantly increases the lifetime of photogenerated charge carriers.

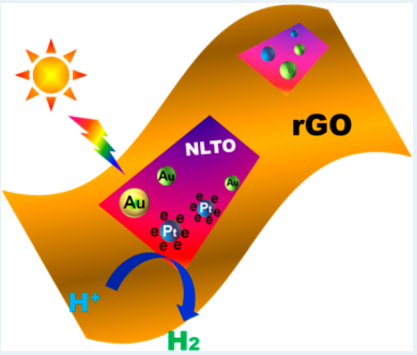

KEYWORDS: *photocatalyst, solar fuel, surface plasmon resonance, $La_2Ti_2O_7$, graphene, hydrogen*

Hydrogen generation by photocatalytic water splitting is a promising technique to provide clean solar fuels to meet the sustainable development needs of the world.[1−8] Semiconductors are the most common materials used for photocatalysts. However, no single semiconductor so far can fulfill all the requirements of photocatalysis. The narrow band gap semiconductors can absorb sunlight in a wide spectral range but suffer from photocorrosion during photocatalysis. In contrast, the wide band gap semiconductors are stable but have a limited light absorption spectral range.[9−12] For example, perovskite lanthanum titanium oxide ($La_2Ti_2O_7$) exhibits good photocatalytic activity toward water splitting under ultraviolet (UV) light irradiation and is very stable.[13−15] However, its wide band gap limits its light absorption spectral range within the UV light region. In addition, it is an ionic conductor at room temperature, which translates to poor electron mobility and a short charge carrier lifetime.

In this paper, the deficits of $La_2Ti_2O_7$ (LTO) will be overcome through materials engineering to allow efficient solar energy harvesting. In order to extend the light absorption spectral range to the visible light region, LTO will be doped with nitrogen to narrow its band gap without introducing midgap states.[13] Furthermore, gold nanoparticles will be deposited on the LTO nanosheet surface to further enhance the light absorption in the visible light region. It has been reported that plasmonic metal nanoparticles can serve as photosensitizers,[5,6,16−24] inducing charge separation in the semiconductor by harvesting light with energy below the band gap of the semiconductor.[16] Plasmonic photosensitizers can absorb sunlight in the visible light region, convert the incident photon's energy to plasmonic energy, and then transfer the plasmonic energy from the metal to the wide band gap semiconductor via the plasmon-induced resonant energy transfer (PIRET)[17] and/or the direct electron transfer (DET) mechanisms,[22−24] enhancing the charge separation in the semiconductor. The interaction of dopants with the plasmonic energy transfer mechanisms remains unknown and thus will be explored in this paper.

In order to compensate the poor lifetime of photogenerated charge carriers, the nitrogen-doped $La_2Ti_2O_7$ (NLTO) nanosheets will also be coupled with gold nanoparticles and reduced graphene oxide (rGO) to form a ternary composite. It has been reported that depositing Au nanoparticles on the semiconductor photocatalyst surface can improve the photocatalytic activity of the semiconductor due to a shift of the flat band potential by Fermi level equilibration.[25−27] Au nanoparticles have also been shown to act as an electron relay in heterostructures, further increasing charge separation.[23,28] In addition, it has been reported that incorporating the reduced graphene oxide (rGO) with a semiconductor can extend the

Received: October 20, 2014
Revised: January 17, 2015
Published: February 12, 2015

DOI: 10.1021/cs5016194
ACS Catal. 2015, 5, 1949−1955

charge carrier lifetime, which enhances the photocatalytic activity.[6]

On the basis of the rationale mentioned above, a Au@Pt-NLTO/rGO composite photocatalyst has therefore been designed to investigate the roles of the nitrogen dopant, the Au nanoparticles, and the rGO in solar energy conversion. The Au@Pt-NLTO/rGO composite exhibited an extended light absorption spectral region up to 600 nm. It is found that the plasmonic energy transfer by PIRET is strongly enhanced after doping, with a transfer efficiency to the LTO of ∼60% of the light absorbed by the plasmon, whereas no plasmonic energy transfer occurs from the plasmonic Au to undoped LTO. The metal nanoparticles also increase the carrier lifetime and reductive power in the doped Au@Pt-NLTO. Under photoexcitation, a ∼2.8-fold increase in the efficiency of charge carrier extraction is measured for Au@Pt-NLTO in comparison to Pt-NLTO. Addition of rGO to Au@Pt-NLTO further increases the efficiency of charge carrier extraction ∼1.8-fold. The combination of metal nanoparticles and rGO therefore gives a 5-fold increase in the efficiency of charge carrier extraction in comparison to Pt-NLTO.

The details of materials synthesis for the four samples Au@Pt-NLTO/rGO, Au@Pt-NLTO, Pt-NLTO, and Au@Pt-LTO/rGO are described in the Supporting Information. The NLTO nanosheets with size 200−300 nm were first synthesized[13] and then decorated with Au or/and Pt nanoparticles on the surface and subsequently combined with rGO to form the Au@Pt-NLTO/rGO composite (Figure 1c). The TEM and HRTEM images of the Au@Pt-NLTO/rGO are shown in Figure 1a,b. The HRTEM image in Figure 1b, taken from the red box area in Figure 1a, clearly shows that both Pt and Au nanoparticles were loaded onto the NLTO nanosheets. The NLTO nanosheet showed a crystal lattice fringe of 0.297 nm, which was attributed to the LTO(−212) facet (JCPDS: 28-0517). The left nanoparticle in Figure 1b showed a Pt(200) facet with a crystal lattice fringe of 0.196 nm (JCPDS: 04-0802). The nanoparticle in Figure 1b exhibited a lattice fringe of 0.232 nm on the Au(111) facet (JCPDS: 04-0784). The morphologies of the Au@Pt-NLTO and Au@Pt-LTO/rGO samples are shown in Figure S1 in the Supporting Information.

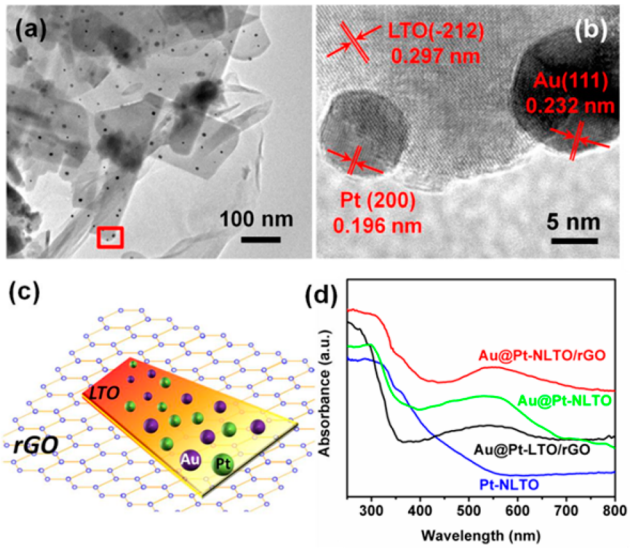

Figure 1. (a) TEM and (b) HRTEM images of the Au@Pt-NLTO/rGO composite, as illustrated in (c). (d) UV−visible spectra of the four samples.

The XPS results are shown in Figure S2 in the Supporting Information. Each of the four samples showed the Pt 4f doublet at 71.0 and 74.1 eV. Except for the Pt-NLTO sample, the other three samples showed the Au 4f doublet at 83.9 and 87.8 eV. The N 1s peak at 398.0 eV appeared in three nitrogen-doped samples, which confirmed that nitrogen atoms were doped into the LTO lattice.[13] The contents of N, Pt, and Au in the samples were calculated as shown in Table S1 in the Supporting Information. The XRD patterns of four samples in Figure S3 in the Supporting Information were consistent with the standard XRD data of LTO (JCPDS: 28-0517), which indicated that the crystal structure of the LTO nanosheets were not altered after nitrogen doping. Only Au@Pt-NLTO/rGO and Au@Pt-LTO/rGO showed the clear rGO peak at 27°. A small XRD peak for Au(111) existed at 38.2° in the XRD patterns of the samples, which were loaded with Au nanoparticles. The Pt(111) peak was consistent in all the four samples. The TEM, XPS, and XRD data confirmed that the Au and Pt nanoparticles were successfully retained in the composite samples after nitrogen doping and hydrothermal synthesis.

Figure 1d and Figure S4 in the Supporting Information show the light absorption spectra. The LTO had an absorption band edge at 3.54 eV (350 nm). Nitrogen doping reduced the band gap to 2.25 eV (550 nm) for NLTO. Our previous study has revealed that nitrogen doping into LTO does not introduce the localized midgap states but instead forms a continuum with the band edge, as reflected in the absorption.[13] After the addition of Au nanoparticles, a localized surface plasmon resonance (LSPR) centered at 550 nm was observed in each sample. The addition of rGO into the samples increased the absorption across the UV−visible range, while the addition of Pt had little effect on the absorption, as shown in Figure 1d and Figure S4.

Hydrogen was generated from water by the photocatalysts under the simulated solar irradiation (Figure 2a). Ethanol was employed as a sacrificial agent to scavenge holes generated in the photocatalytic water reduction. All four samples showed stable and recyclable photocatalytic properties in three continuous runs of photocatalytic hydrogen generation (Figure S5 in the Supporting Information). The average rates of photocatalytic hydrogen generation and the specific surface areas of the four samples were collected in Table S2 in the Supporting Information, showing the difference in photocatalytic activity between samples was not caused by a difference in the specific surface area. The undoped Au@Pt-LTO/rGO sample showed the lowest hydrogen production rate (Figure 2a). After nitrogen doping, the Pt-NLTO showed a greater hydrogen production rate than the Au@Pt-LTO/rGO due to the extended light absorption range. Loading of the Au nanoparticles to the Pt-NLTO increased the hydrogen production rate by ∼150%. After addition of rGO to the Au@Pt-NLTO sample, the hydrogen production rate further increased by 250% in comparison to the Pt-NLTO alone. The hydrogen production rate showed that the doping and plasmonic enhancements acted synergistically, enhancing the performance beyond that of the undoped Au@Pt-LTO/rGO sample.

In order to understand the underlying mechanism of photocatalysis enhancement by nitrogen doping and loading of Au nanoparticles and rGO, the photocatalyst powder was deposited on the fluorine-doped tin oxide (FTO) substrate to act as the photoelectrode in a photoelectrochemical cell (PEC),

DOI: 10.1021/cs5016194
ACS Catal. 2015, 5, 1949−1955

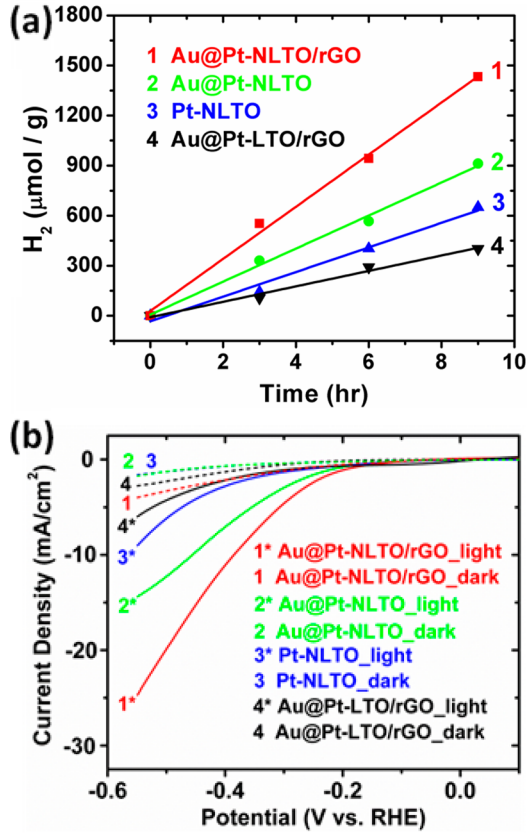

Figure 2. (a) Hydrogen generated by the photocatalysts. (b) $J-V$ curve plotting the photocurrent density as a function of the applied potential.

and then the photoelectrochemical behavior of the photoelectrode was investigated. The $J-V$ curve (photocurrent density vs the applied potential) in Figure 2b shows that the photocurrent density followed the same increasing trend as the hydrogen production rate (Figure 2a). The photocurrents of the LTO, NLTO, Au-LTO, and Au-NLTO are shown in Figure S4 in the Supporting Information for reference.

When the Au nanoparticles are brought into contact with the LTO, a Schottky barrier will form, altering the band structure near the semiconductor surface and changing the band alignment,[25−27] as shown in the inset of Figure 3b. This results in a change in the flat band potential, which is the potential offset at the semiconductor/electrolyte interface, and a change in the onset potential due to the shift in the Fermi level (inset in Figure 3a,b).[25−27] The change in Fermi level from the Au/NLTO interface reduces the overpotential, as reflected in the shift of the onset potential.[29,30] The onset potential for the Pt-NLTO and the Au@Pt-NLTO samples were −0.27 and −0.21 V (vs RHE), respectively.

The flat band potential can be measured using the Mott−Schottky analysis as shown in Figure 3 and Figure S6 in the Supporting Information. The intercept gives the flat band potential, as outlined in the Supporting Information and eq S3. When the Pt-NLTO is excited, the flat band potential becomes more negative and the slope decreases due to the increased charge density under illumination (Figure 3a). The flat band potential becomes slightly more negative under illumination because the band bending at the semiconductor/electrolyte interface pushes electrons away from the interface while attracting holes (inset in Figure 3a), increasing the band bending while keeping the Fermi level equilibration.[25−27] The shift was small in the NLTO alone because of the large recombination of electron−hole pairs at the semiconductor surface.[25−27] When Au was added to the Pt-NLTO, the photogenerated electrons could transfer from the semiconductor to the Au nanoparticle, which allowed a more negative shift of the flat band potential, reducing the charge recombination. In other words, the Fermi equilibration effect of Au nanoparticles can increase the efficiency of charge carrier extraction. It can be seen that from Figure 3b and Table S3 in the Supporting Information that the flat band potentials were −0.71 and −0.57 V for Au@Pt-NLTO and Pt-NLTO, respectively. It is interesting that the addition of rGO did not affect the flat band potential.

The effect of the Fermi equilibration and rGO on the charge carrier lifetime was evaluated by recording the transient photocurrent at a bias of −0.25 V vs the reversible hydrogen electrode (RHE) (Figure S7 in the Supporting Information). To evaluate the charge recombination behavior quantitatively, a normalized parameter (D) is introduced according to eq S5 in the Supporting Information.[31] The normalized plots of ln D versus time (t) are plotted in Figure 3d. The time at ln $D = -1$ is defined as the transient time constant (τ) to allow comparison of the charge carrier lifetime. τ was 23.3, 10.8, 9.1, and 17.1 s for the Au@Pt-NLTO/rGO, Au@Pt-NLTO, Pt-NLTO, and Au@Pt-LTO/rGO, respectively. As expected, Figure 3b shows that an increase in the flat band potential due to Fermi level equilibration in the Au@Pt-NLTO increased the charge carrier lifetime over that of the Pt-NLTO. Further, rGO effectively transported the charge carriers away from the LTO, increasing the charge carrier lifetime in both the doped and undoped samples. The increase in carrier lifetime was larger when rGO was present, although the flat band potential was not affected (Figure 3), suggesting the Au nanoparticles may act as electron relays, increasing the overall charge extraction into the rGO layer.

In the present work, the Au nanoparticle not only leads to a shift in the flat band potential but also acts as a plasmonic photosensitizer to enhance the photocatalytic hydrogen evolution. To separate the plasmonic enhancement effect from the increased charge carrier lifetime caused by Fermi level equilibration, the IPCE spectrum was measured at a bias of −0.25 V vs RHE (Figure 4a and Figure S4d in the Supporting Information). It can be seen that the spectral utilization increased with N doping, shifting the band edge from 325 nm (for Au@Pt-LTO/rGO) to 525 nm (for Pt-NLTO), which was in agreement with the absorbance (Figure 1d). The same trend was seen for addition of Au to LTO and NLTO, which confirmed that the IPCE of Au@Pt-LTO/rGO can be used as a baseline for performance. After addition of the Au nanoparticle to NLTO and Pt-NLTO, the IPCE curves show that the photoconversion was extended to 600 nm for both samples (Figure 4a and Figure S4d). Below the 525 nm band edge of the NLTO, the IPCE was much higher than those samples without Au nanoparticles (Figure 4a and Figure S4d).

As discussed previously, plasmonic energy can transfer from the metal to semiconductor via either a DET or PIRET process (Figure S9 in the Supporting Information), inducing the charge separation in the semiconductor. In DET, the spectral enhancement follows the absorption of the plasmon, with a strength dependent on band alignment.[17,32] In PIRET, the spectral enhancement and strength of transfer both follow the spectral overlap (Figure S8 in the Supporting Information).[16,17]

DOI: 10.1021/cs5016194
ACS Catal. 2015, 5, 1949−1955

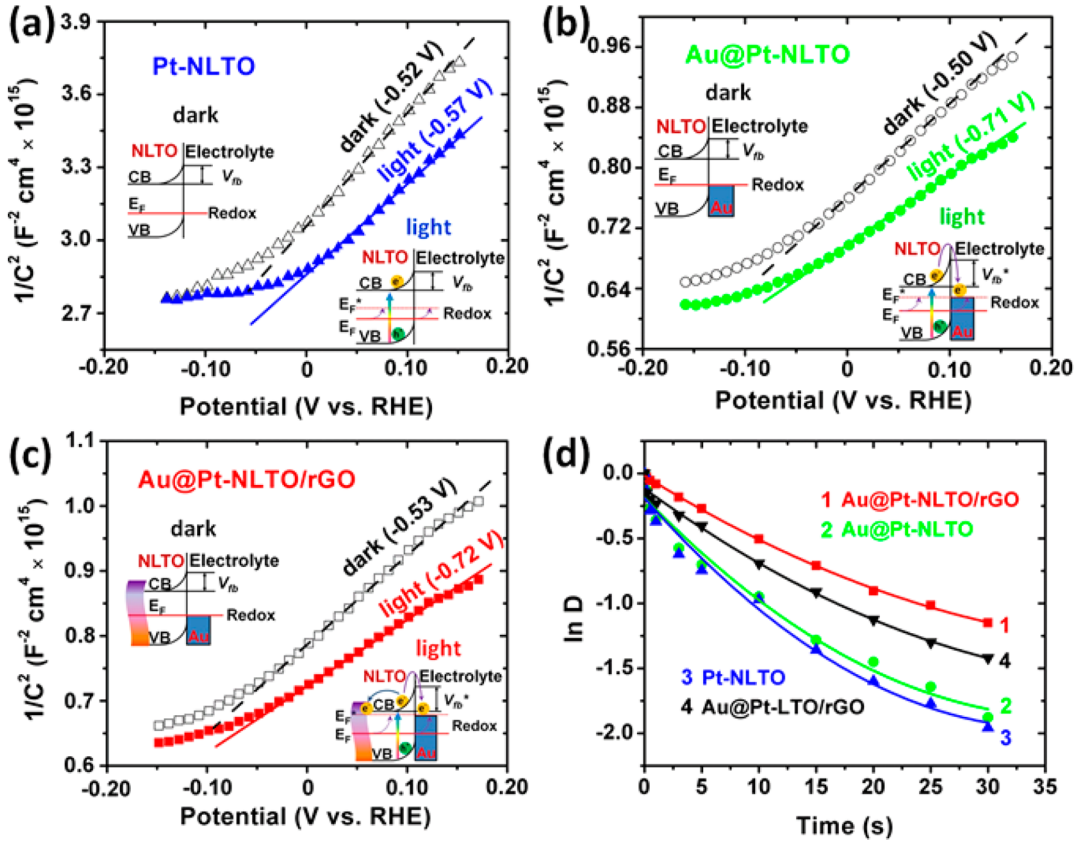

Figure 3. Mott−Schottky plots for (a) Pt-NLTO, (b) Au@Pt-NLTO, and (c) Au@Pt-NLTO/rGO. The flat band potential shifts under illumination due to the shift in the excited state Fermi level (inset (a)). This effect is amplified at the Au/NLTO interface since excited carriers migrate into the Au, increasing the lifetime (inset (b)). The shift in the flat band potentials increase the carrier lifetime, as measured by the normalized transient conductivity (d).

For the Au@Pt-LTO/rGO composite, the plasmonic Au nanoparticle can absorb light around 550 nm (Figure 1d). However, its IPCE at around 550 nm was 0 (Figure 4a); given that no spectral overlap was present for PIRET, this implied that DET was weak. In the Au@Pt-NLTO/rGO composite, the absorption band of N-doped LTO was overlapped with the LSPR band of Au nanoparticles (Figures 1d and 4d), leading to IPCE enhancement (Figure 4a). Since the photoconversion enhancement followed the spectral overlap and not the absorption of the plasmon, the dominant plasmonic energy transfer mechanism was most likely PIRET instead of DET.[16,17] The same trend was seen in LTO and NLTO without the Pt and rGO (Figure S4 in the Supporting Information), which confirmed that these materials did not affect the plasmonic energy transfer or otherwise extend the photoconversion range. The lack of DET may be due to a large Schottky barrier present at the interface or poor charge transfer kinetics from the plasmon to the LTO due to the ionic conductivity of LTO. PIRET is a nonradiative energy transfer mechanism.[17] Therefore, charge separation is not affected by the poor ionic conductivity, with the charge carriers being excited identically as under incident illumination.

Generally, a plasmon dephases and generates a hot electron/hole pair within ∼5−10 fs. In this case, the PIRET process still can occur. While the dephasing time of the plasmon is short, using a basic RET type theory gives the transfer rate as

$$\frac{1}{\tau_{\mathrm{PIRET}}} \approx \frac{1}{\tau_{\mathrm{plasmon}}}\left(\frac{R_0}{R}\right)^6 \quad (1)$$

While this is based on an incoherent energy transfer process, it still shows that if R, the distance from the metal to the semiconductor, is less than R_0, usually 5−10 nm given the large dipole moment of the plasmon, the transfer rate will be quicker than the lifetime of the plasmon. Further, when the coherence of the plasmon is taken into account, it is found that transfer on these time scales can actually be more efficient than if incoherent effects are included,[33] as is now known for RET in photosynthesis.[34] Therefore, the short dephasing time of the plasmon can actually increase the energy transfer efficiency.

The overall hydrogen generation rate or photocurrent is proportional to the number of photogenerated charge carriers ($\alpha(h\nu)$) times the efficiency of carrier extraction (η_{lifetime}), which is determined by the charge recombination, migration, and surface kinetics:

$$\text{yield} \approx \alpha(h\nu) \times \eta_{\mathrm{lifetime}} \quad (2)$$

The presence of rGO and the Fermi level equilibration effect of Au nanoparticles are expected to enhance the charge carrier extraction (η_{lifetime}), not the number of photogenerated charge carriers ($\alpha(h\nu)$). Therefore, the IPCE enhancement from these effects is independent of the wavelength of incident light. In other words, the IPCE enhancement can be determined via multiplying by a constant factor. This behavior is seen by comparing the IPCE before and after the addition of rGO and

DOI: 10.1021/cs5016194
ACS Catal. 2015, 5, 1949−1955

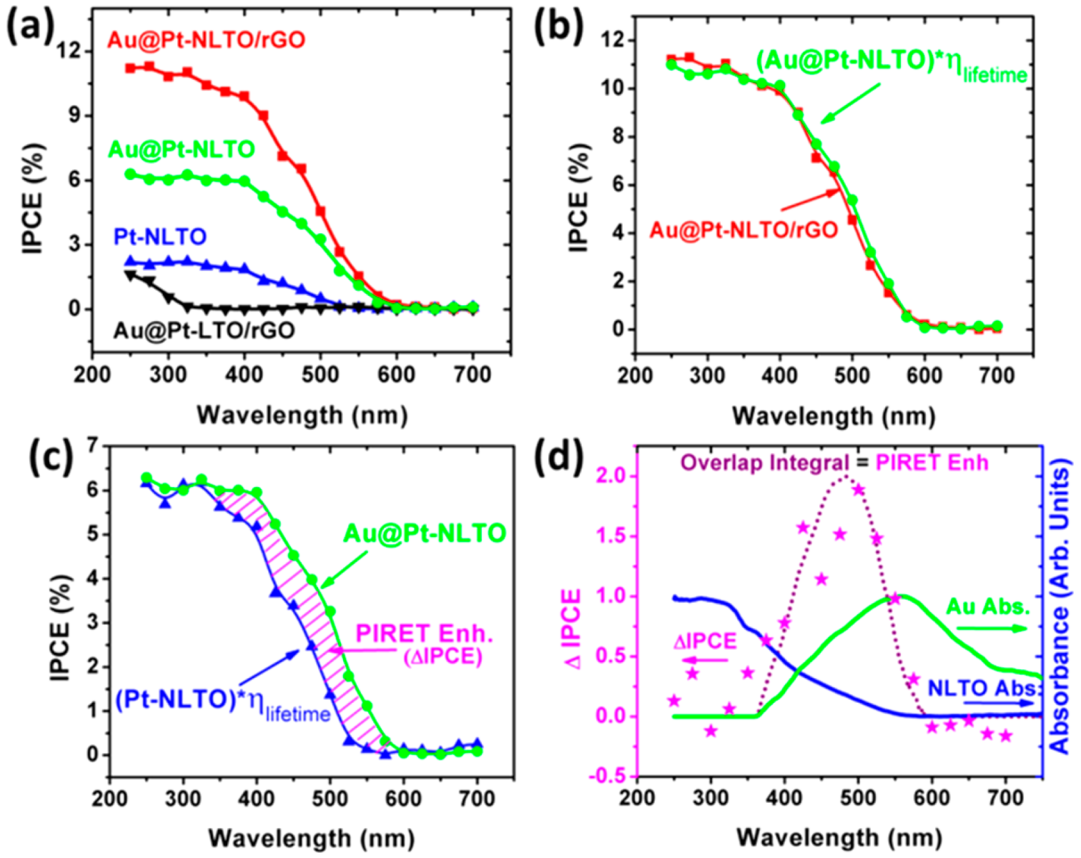

Figure 4. (a) IPCE spectra. (b) rGO does not change the spectral utilization of the NLTO and acts only to increase the IPCE by the constant factor η_{lifetime}. (c) Plasmonic energy transfer can increase the spectral utilization of the NLTO in addition to the factor η_{lifetime}, as shown by the hatched region. (d) The increase in the spectral utilization in the IPCE is seen to be proportional to the overlap integral between the Au and NLTO, proving the enhancement is from PIRET.

Au nanoparticles (Figure 4b,c). When Au is added to the Pt-NLTO, it can increase the charge extraction by Fermi level equilibration and charge trapping. These enhancements only affect the lifetime of photogenerated charge carriers, not the carrier generation versus the wavelength. Hence, the IPCE of Au@Pt-NLTO above the band edge is equal to that of Pt-NLTO times the increase in η_{lifetime} (Figure 4c), which is equal to ∼2.8 times. Similarly, when rGO is added to the Au@Pt-NLTO, the charge extraction further increases by a factor of ∼1.8 (Figure 4b), although no spectral extension is seen for the addition of rGO into the undoped Au@Pt-LTO. The combination of Au and rGO increases the charge extraction efficiency by ∼5 times that of the Pt-NLTO alone. The constant increase also rules out the light-scattering enhancement by rGO, which would also enhance above the band edge but would depend on the wavelength of incident light.

An increase in the charge extraction efficiency completely describes the IPCE enhancement by the presence of rGO (Figure 4b). However, an increase in charge extraction efficiency only partially describes the IPCE enhancement by the presence of Au nanoparticles (Figure 4c). The remaining increase in spectral conversion on comparison of the plasmonic sample with the nonplasmonic sample is shown by the hatched section in Figure 4c for Au@Pt-NLTO versus Pt-NLTO and for Au@Pt-NLTO/rGO versus Pt-NLTO in Figure S9 in the Supporting Information. This enhancement was due to a PIRET-induced increase in the number of photogenerated charge carriers ($\alpha(h\nu)$) versus the wavelength of incident light.

Figure 4d shows the extracted spectral enhancement of the IPCE, represented as

$$\Delta\alpha(h\nu) \approx \Delta\text{IPCE} = \text{IPCE}_{\text{Au@NLTO}} - \text{IPCE}_{\text{NLTO}} \quad (3)$$

The enhancement $\Delta\alpha_{\text{PIRET}}(h\nu)/\alpha_0(h\nu)$ will be proportional to the overlap integral, which is itself proportional to the overlap of the absorption band of NLTO with the LSPR band of Au nanoparticles:

$$\Delta\alpha(h\nu) \approx \int \sigma_{\text{NLTO}}(\lambda)\cdot F_{\text{Au}}(\lambda)\cdot\lambda^4 \, \mathrm{d}\lambda \quad (4)$$

where $\sigma_{\text{NLTO}}(\lambda)$ is the absorption cross section of the NLTO and the emission of the plasmon $F_{\text{Au}}(\lambda)$ can be approximated as the absorption cross section $\sigma_{\text{Au}}(\lambda)$ of the plasmon. The absorption cross section of the plasmon is extracted from Figure 1d by subtracting the absorption of the Pt-NLTO from that of the Au@Pt-NLTO sample and then fitting the LSPR peak with a Gaussian to remove the absorption due to the interband transition in Au. If DET were present, the enhancement would only follow $\sigma_{\text{Au}}(\lambda)$ and not the overlap integral.

The resulting overlap integral was calculated as shown in Figure 4d and is seen to fit the spectral enhancement of the IPCE excellently. This further proves that PIRET is the underlying mechanism of carrier creation enhancement and that the interaction of the doping and plasmonics extends the spectral utilization of the semiconductor. The total enhancement over the measured solar spectrum

DOI: 10.1021/cs5016194
ACS Catal. 2015, 5, 1949−1955

$$\frac{\Delta\alpha_{\mathrm{PIRET}}(h\nu)}{\alpha_0(h\nu)} = \int \Delta\mathrm{IPCE}_{\mathrm{PIRET}}(h\nu) / \int \mathrm{IPCE}_{\mathrm{NLTO}}(h\nu) \quad (5)$$

can be calculated by integrating the corresponding IPCE spectrum. This gives the enhancement as ~60% for the Au@Pt-NLTO (Figure 4d) and ~68% for the Au@Pt-NLTO/rGO (Figure S9 in the Supporting Information). Further, using the measured absorption, the maximum possible enhancement by PIRET can be estimated by calculating the increase in the IPCE if all the energy absorbed by the plasmonic Au is transferred to the NLTO

$$\frac{\Delta\alpha_{\mathrm{total}}(h\nu)}{\alpha_0(h\nu)} = \left(\int \Delta\sigma_{\mathrm{Au@NLTO}} \cdot I_{\mathrm{SUN}} - \int \sigma_{\mathrm{NLTO}} \cdot I_{\mathrm{SUN}}\right) / \int \sigma_{\mathrm{NLTO}} \cdot I_{\mathrm{SUN}} \quad (6)$$

where I_{SUN} is the AM1.5G spectrum. If the measured enhancement is divided by this maximum value, calculated to be ~100% of the NLTO IPCE, the value is equal to the PIRET efficiency, or how well PIRET transfers absorbed energy in the Au to the NLTO. Using this procedure, the PIRET transfer efficiency $((\int \Delta\alpha_{\mathrm{PIRET}}(h\nu))/(\int \Delta\alpha_{\mathrm{total}}(h\nu)))$ was found to be ~60% for the Au@Pt-NLTO. This implies that 60% of the solar energy absorbed by the LSPR is being transferred into the NLTO and converted into a photocurrent.

In conclusion, the photocatalytic hydrogen generation rate of the LTO nanosheets was improved by nitrogen doping and the formation of a heterojunction with the Au nanoparticles and the rGO nanosheets. The addition of rGO to the photocatalyst increased the charge extraction by a factor of ~1.8, although rGO did not affect the charge separation. Both nitrogen doping and the presence of surface Au nanoparticles led to a shift in the flat band potential due to Fermi level equilibration, which increased the charge carrier lifetime, leading to an increase in the charge extraction efficiency. When the Au nanoparticles were absent in the photocatalyst, nitrogen doping acted alone to extend the light absorption range of the photocatalyst to 550 nm. When the Au nanoparticles were present in the photocatalyst, nitrogen doping and plasmonics interacted with each other, which resulted in the synergistic enhancement of photocatalysis under solar radiation up to 600 nm. Nitrogen doping led to the spectral overlap of the absorption band of NLTO with the LSPR band of Au nanoparticles, thereby enabling the PIRET process to transfer the plasmonic energy from the Au nanoparticle to NLTO, leading to charge separation in NLTO. For the Au-LTO composite, although the plasmonic Au nanoparticles can absorb light, no enhancement occurs because of the lack of spectral overlap and weak plasmonic electron transfer. The results show that the coupling of plasmonic metals with doping can address both spectral utilization and carrier lifetime/extraction, the major weaknesses of current photocatalyst for solar-to-hydrogen conversion.

■ ASSOCIATED CONTENT

Supporting Information

The following file is available free of charge on the ACS Publications website at DOI: 10.1021/cs5016194.

TEM, XPS, XRD characterizations, photocatalytic activity stability, and transient absorption analysis (Figures S1–S9 and Tables S1–S3) (PDF)

■ AUTHOR INFORMATION

Corresponding Author

*N.W.: fax, +1-304-293-6689; tel, +1-304-293-3326; e-mail, nick.wu@mail.wvu.edu.

Notes

The authors declare no competing financial interest.

■ ACKNOWLEDGMENTS

This work was supported by the National Science Foundation (CBET-1233795) and the Army Research Laboratory (W911NF-14-2-0116). S.K.C. was supported by an NSF Graduate Research Fellowship under Grant 1102689. The resource and facilities were partially supported by the NSF (EPS 1003907). The use of a WVU shared facility is appreciated.

■ REFERENCES

(1) Fujishima, A.; Honda, K. *Nature* **1972**, *238*, 37–38.
(2) Kudo, A.; Miseki, Y. *Chem. Soc. Rev.* **2009**, *38*, 253–278.
(3) Zou, Z. G.; Ye, J. H.; Sayama, K.; Arakawa, H. *Nature* **2001**, *414*, 625–627.
(4) Chen, X. B.; Shen, S. H.; Guo, L. J.; Mao, S. S. *Chem. Rev.* **2010**, *110*, 6503–6570.
(5) Awazu, K.; Fujimaki, M.; Rockstuhl, C.; Tominaga, J.; Murakami, H.; Ohki, Y.; Yoshida, N.; Watanable, T. *J. Am. Chem. Soc.* **2008**, *130*, 1676–1680.
(6) Liu, Z.; Hou, W.; Pavaskar, P.; Aykol, M.; Cronin, S. B. *Nano Lett.* **2011**, *11*, 1111–1116.
(7) Maeda, K.; Domen, K. *J. Phys. Chem. Lett.* **2010**, *1*, 2655–2661.
(8) Laursen, A. B.; Kegnas, S.; Dahl, S.; Chorkendorff, I. *Energy Environ. Sci.* **2012**, *5*, 5577–5591.
(9) Wang, X. C.; Maeda, K.; Thomas, A.; Takanabe, K.; Xin, G.; Carlsson, J.; Domen, K.; Antonietti, M. *Nat. Mater.* **2009**, *8*, 76–80.
(10) Abe, R.; Higashi, M.; Domen, K. *J. Am. Chem. Soc.* **2010**, *132*, 11828–11829.
(11) Kay, A.; Cesar, I.; Gratzel, M. *J. Am. Chem. Soc.* **2006**, *128*, 15714–15721.
(12) Guo, J. J.; Li, Y.; Zhu, S. M.; Chen, Z. X.; Liu, Q. L.; Zhang, D.; Moon, W. J.; Song, D. M. *RSC Adv.* **2012**, *2*, 1356–1363.
(13) Meng, F. K.; Hong, Z. L.; Arndt, J.; Li, M.; Zhi, M. J.; Yang, F.; Wu, N. Q. *Nano Res.* **2012**, *5*, 213–221.
(14) Hu, S.; Jia, L.; Chi, B.; Pu, J.; Jian, L. *J. Power Sources* **2014**, *266*, 304–312.
(15) Maeda, K. *J. Photochem. Photobiol. C* **2011**, *12*, 237–268.
(16) Cushing, S. K.; Wu, N. Q. *Interface* **2013**, *22*, 63–67.
(17) Cushing, S. K.; Li, J. T.; Meng, F. K.; Senty, T. R.; Suri, S.; Zhi, M. J.; Li, M.; Bristow, A. D.; Wu, N. Q. *J. Am. Chem. Soc.* **2012**, *134*, 15033–15041.
(18) Long, J.; Chang, H.; Gu, Q.; Xu, J.; Fan, L.; Wang, S.; Zhou, Y.; Wei, W.; Huang, L.; Wang, X.; Liu, P.; Huang, W. *Energy Environ. Sci.* **2014**, *7*, 973–977.
(19) Lin, H.; Ding, L.; Pei, Z.; Zhou, Y.; Long, L.; Deng, W.; Wang, X. *Appl. Catal. B: Environ.* **2014**, *160–161*, 98–105.
(20) Thomann, I.; Pinaud, B. A.; Chen, Z.; Clemens, B. M.; Jaramillo, T. F.; Brongersma, M. L. *Nano Lett.* **2011**, *11*, 3440–3446.
(21) Hu, C.; Peng, T.; Hu, X.; Nie, Y.; Zhou, X.; Qu, J.; He, H. *J. Am. Chem. Soc.* **2010**, *132*, 857–862.
(22) Tian, Y.; Tatsuma, T. *J. Am. Chem. Soc.* **2005**, *127*, 7632–7637.
(23) Li, J. T.; Cushing, S. K.; Zheng, P.; Senty, T.; Meng, F. K.; Manivannan, A.; Wu, N. Q. *J. Am. Chem. Soc.* **2014**, *136*, 8438–8449.
(24) Mubeen, S.; Hernandez-Sosa, G.; Moses, D.; Lee, J.; Moskovits, M. *Nano Lett.* **2011**, *11*, 5548–5552.
(25) Subramanian, V.; Wolf, E. E.; Kamat, P. V. *J. Am. Chem. Soc.* **2004**, *126*, 4943–4950.
(26) Jakob, M.; Levanon, H.; Kamat, P. V. *Nano Lett.* **2003**, *3*, 353–357.

DOI: 10.1021/cs5016194
ACS Catal. 2015, 5, 1949–1955

(27) Rosseler, O.; Shankar, M. V.; Karkmaz-Le Du, M.; Schmidlin, L.; Keller, N.; Keller, V. J. *J. Catal.* **2010**, *269*, 179−190.
(28) Tada, H.; Mitsui, T.; Kiyonaga, T.; Akita, T.; Tanaka, K. *Nat. Mater.* **2006**, *5*, 782−786.
(29) Sivula, K.; Le-Formal, F.; Michael, G. *ChemSusChem* **2011**, *4*, 432−449.
(30) Katz, M.; Riha, S.; Jeong, N.; Martinson, A.; Farha, O.; Hupp, J. *Coord. Chem. Rev.* **2012**, *256*, 2521−2529.
(31) Tafalla, D.; Salvador, P.; Benito, R. *J. Electrochem. Soc.* **1990**, *137*, 1810−1815.
(32) Govorov, A. O.; Zhang, H.; Gun'ko, Y. K. *J. Phys. Chem. C* **2013**, *117*, 16616−16631.
(33) Jang, S.; Cheng, Y. C.; Reichman, D. R.; Eaves, J. D. *J. Chem. Phys.* **2008**, *129*, 101104.
(34) Scholes, G. D. *J. Phys. Chem. Lett.* **2010**, *1*, 2−8.

NOTE ADDED AFTER ASAP PUBLICATION

After this paper was published ASAP on February 24, 2015, a correction was made to Figure 2a. The corrected version was reposted March 6, 2015.

DOI: 10.1021/cs5016194
ACS Catal. 2015, 5, 1949−1955